THE AMERICAN SOCIETY OF MECHANICAL ENGINEERS
Three Park Avenue, New York, N.Y. 10016-5990

99-GT-225

APPLICATION OF PERTURBATION METHODOLOGY AND DIRECTIONAL FILTERING FOR EARLY ROTOR CRACK DETECTION

Paul Goldman
Agnes Muszynska
Donald E. Bently
Kenwood P. Dayton
BRDRC
1711 Orbit Way, Bldg. 1
Minden, NV 89423, USA

Mauro Garcin
Politecnico di Torino
Corso Duca Degli Abruzzi, 24
10129 Torino, Italy

ABSTRACT

This paper documents analytical and experimental research of the lateral and torsional responses of a cracked rotor to different types of excitation. The experimental research has been performed on a rotor rig, which emulate a turbogenerator. It includes driving motor coupled to the main rotor, a lateral nonsynchronous perturbation device, and a generator with an electrical field consisting of a constant component (constant torsional load) and a sinusoidal component, provided by a signal generator. The generator was used as a torsional nonsynchronous perturbation device. The midspan of the rotor was modified so that a section could be changed starting with a circular cross-section (undamaged rotor) to the cross-section with transverse crack. The lateral and torsional responses have been measured at two axial locations. The obtained lateral data was processed using directional filtering into forward and reverse components of the corresponding filtered elliptical orbits. The forward component of the lateral response to nonsynchronous perturbation allows to identify overall stiffness reduction and rotating stiffness asymmetry introduced by the change in midspan rotor cross-section, while the reverse component largly depends on the support asymmetry. The nonsynchronous torsional excitation allows identify of the system torsional dynamic stiffness and it's reduction due to the crack. The ratio of the filtered to 1x or to the perturbation frequency rotor responses at two axial locations was considered as an indicator of a lateral mode shape change due to the crack. The experimental results are compared with the analytical model of the rotor response, which was obtained by the application of a perturbation method of small parameter to the system of nonlinear equations. The equations describe the rotor system with four lateral (two displacements and two inclination angles) and two torsional degrees of freedom.

1. INTRODUCTION

Over the years many papers on early detection of shaft cracks have been published. The continuing interest of scientists and engineers is stimulated by a severity of the malfunction in terms of lost and safety. A relatively high frequency of crack occurance also motivates a continued investigation into the subject. According to Bently, Muszynska (1986) during a period of 10 years at least 28 rotor failures due to cracks were documented in the USA power industry.

Dimentberg (1945) was apparently the first to report the effect of the rotating stiffness asymmetry on the shaft lateral vibration. Henry and Okah-Avae (1976) performed a computer study where the weight of the rotor was reported to be responsible for the 2x resonance. Mayes and Davis (1976) studied the behavior of a cracked shaft model which took into account opening and closing of the crack as a stiffness step-function. Gasch (1976) modeled the breathing crack by a spring-loaded hinge, and performed a computer simulation which showed a subharmonic resonance. Grabowski (1979) used a modal approach to the problem. He developed a theoretical model of the crack mechanism, which showed a good correlation with static experiments, and used it in a dynamic model of the rotor. Inagaki, Kanaki and Shiraki (1979) applied the transfer matrix method. They modeled the breathing crack as a step-

Presented at the International Gas Turbine & Aeroengine Congress & Exhibition
Indianapolis, Indiana — June 7–June 10, 1999

function for the bending moment and applied the Fourier series expansion to find the solution. Muszynska (1982) considered both gaping and breathing cracks and investigated the interaction between rotating and stationary stiffness asymmetries. Nelson and Nataraj (1986) investigated analytically the spectrum change due to the nonlinearities introduced by cracks. Bently and Muszynska (1986) emphasized the importance of the observation of the rotor 1x and 2x filtered response vector changes for early crack detection, including not only amplitudes, but also phases. A significant number of papers were published on the finite element modeling of the cracked shafts, for example: Chen and Wang (1986), Schmallhorst and Dirr (1987). The free mode shape change due to the crack has been investigated by Goldman et al. (1996).

In comparison to the great number of papers on the lateral vibration, which is considered as the major effect of the cracked rotors, the number of papers on the torsional vibration due to cracks is much less. Among them Dimarogonas and Massouros (1981) reported the first torsional natural frequency reduction due to the transverse crack. Christides and Barr (1986) developed partial differential equations for the torsional vibration of the cracked shaft under the assumptions which uncoupled lateral and torsional modes. The finite element model was applied to the modeling of the torsional vibration of the cracked shafts in the paper by Chen and Wang (1986). Papadopoulos and Dimarogonas (1989) derived the cross-coupled local stiffness matrix, which resulted in the lateral/torsional cross-coupling effect. Muszynska, Goldman and Bently (1992) and Bently, Goldman Muszynska (1994) investigated analytically and experimentally the other lateral/torsional cross-coupling mechanism (due to the combination of the unbalance, shaft stiffness asymmetry, and radial side load).

In spite of number of papers and recommendations on the early crack detection, shafts keep breaking, sometimes without exhibiting detectable changes in some of the recommended parameters. That brings a conclusion that just a passive vibration monitoring is not always sufficient. An active testing for early shaft crack detection might be required in some cases. This paper presents the active testing technology and dicusses analytical and experimental results on the cracked rotor lateral and torsional responses to different types of excitations: unbalance, constant radial load, lateral and torsional nonsynchronous harmonic excitations.

2. EXPERIMENTAL SETUP

The schematic diagram of the experimental setup is shown in Fig. 1. The experimental rotor rig consists of the main rotor with the interchangeable midspan, and the two perturbation devices.

The main rotor includes a variable speed, $1/10$ horsepower electric motor, which is connected to the main shaft through a flexible coupling. The main shaft is a 10 mm outside diameter steel rod cut into two sections. The inner end of each section is female threaded to accept the male threads of the midspan. There are two types of midspans manufactured for the experimentation (undamaged and cracked), each fabricated from the same material as the main shaft. Berg® Quick-2-Clamp™ clamps are used at the junctions of the main rotor and midspan ends to reduce asymmetry and increase the stiffness of the rotor at the junctions. Three bearings, 1 bronze bushing bearing (B1) and 2 rolling element bearings (B2 & B3) support the main rotor. The bronze bushing bearing is used to introduce damping to the system. The rolling element bearings are used to increase the stiffness of the rotor.

In order to limit the number of lateral vibration modes at the midspan to a single mode, placing it between bearings B2 and B3 laterally restricts the outboard disk, D2. The masses used in this case are both made of steel with dimensions of 4.9" diameter, .5" thickness, and approximately 1210 grams. The inboard mass was placed close to the midspan as possible such that the natural frequency of the system's lateral vibration would coincide with the natural frequency of the system's torsional vibration. A spring stand was placed near the mass at the inboard side of the midspan to control constant radial loading of the system.

Two torsional measurement gears, G_1 and G_2, were located at each end of the main rotor near each of the masses. Placing the gears near the masses ensures that the torsional measurements will not be taken near a nodal point, thus increasing the signal to noise ratio of the measurements. Two sets of lateral proximity probes are used to take lateral vibration measurements at the outboard side of the midspan and near the inboard disk, D1. The proximity probes are standard Bently Nevada Corporation 5 mm type probes. The main rotor as well as the lateral perturbator has independent Keyphasor™ signals to provide a corresponding phase reference. The phase reference for the nonsynchronous torsional perturbation is the transistor-to-transistor logic (TTL) pulse from the function generator.

The nonsynchronous lateral excitation is provided by a constant force perturbator located on the midspan section. The constant force perturbator device is based on the concept if constant elastic eccentricity. Electric motors separate from the main drive motor drives the constant force perturbator through a toothed drive belt. The teeth on the drive belt prevent slip between the drive motor and the constant force perturbator giving more accurate phase reference.

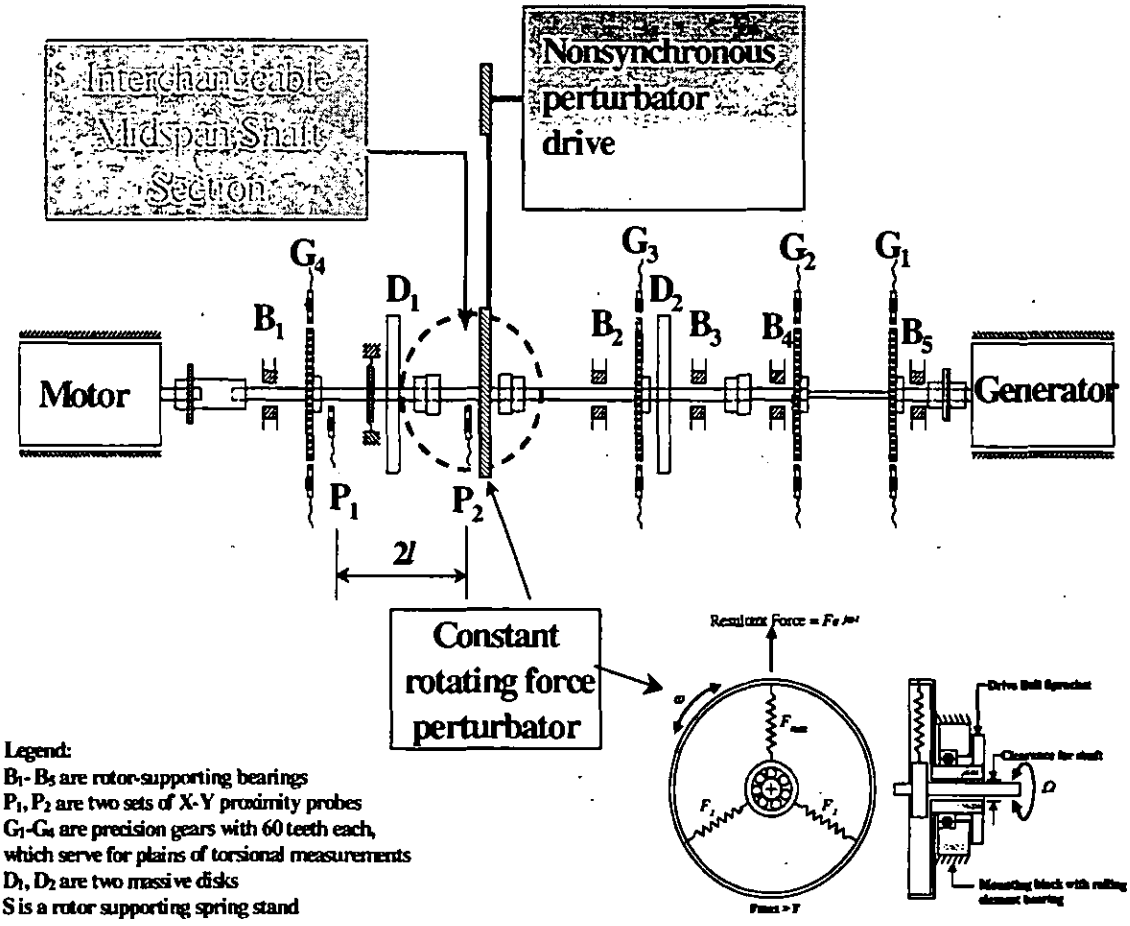

Figure 1. Schematic of the experimental setup.

Torsional perturbation is applied by a torsional perturbator assembly, which is attached to the outboard end of the main rotor using a Berg® Quick-2-Clamp™ clamp. The torsional perturbator consists of two torsional measurement gears fixed to a 10 mm shaft. Two rolling element bearings, B4 & B5 support the shaft. In order to increase the torsional response between the two gears, G_3 & G_4, and proportionally increase the signal to noise ratio, the shaft is reduced to 5 mm. The shaft is connected to an electric motor, identical to the drive motor, through a torsionally rigid coupling. The electric motor acts as a generator, since it is being driven by the main rotor, and serves as the source of the nonsynchronous torsional perturbation. Modifying the field of the generator by a harmonic signal, results in a variable torque being applied to the main rotor through the shaft of the torsional perturbator assembly. The actual resulting torque input into the main rotor system is the response measured between gears G_3 and G_4 multiplied by the stiffness of the reduced diameter section between the two gears.

2. MATHEMATICAL MODEL

The physical model of the rotor presented in Fig. 2, consists of two rigid bodies. The first rigid body is considered having two angular (χ-angle of yaw and ψ -angle of pitch), two displacement (x and y) and one torsional (ϕ) degrees of freedom. It models the part of the main rotor (see Fig.1) between two sets of proximity probes P_1 and P_2. Five measurements: four laterals (from two sets of probes P_1 and P_2) and one torsional (from the gear G_1)- determine the described five degrees of freedom of this rigid body. It is supported at the driving end by an anisotropic stationary stiffness element with major stiffness axes X and Y and corresponding stiffnesses $(K_{s0} - \Delta K_s)/2$ and $(K_{s0} + \Delta K_s)/2$ (ΔK_s is a measure of the support stiffness anisotropy).

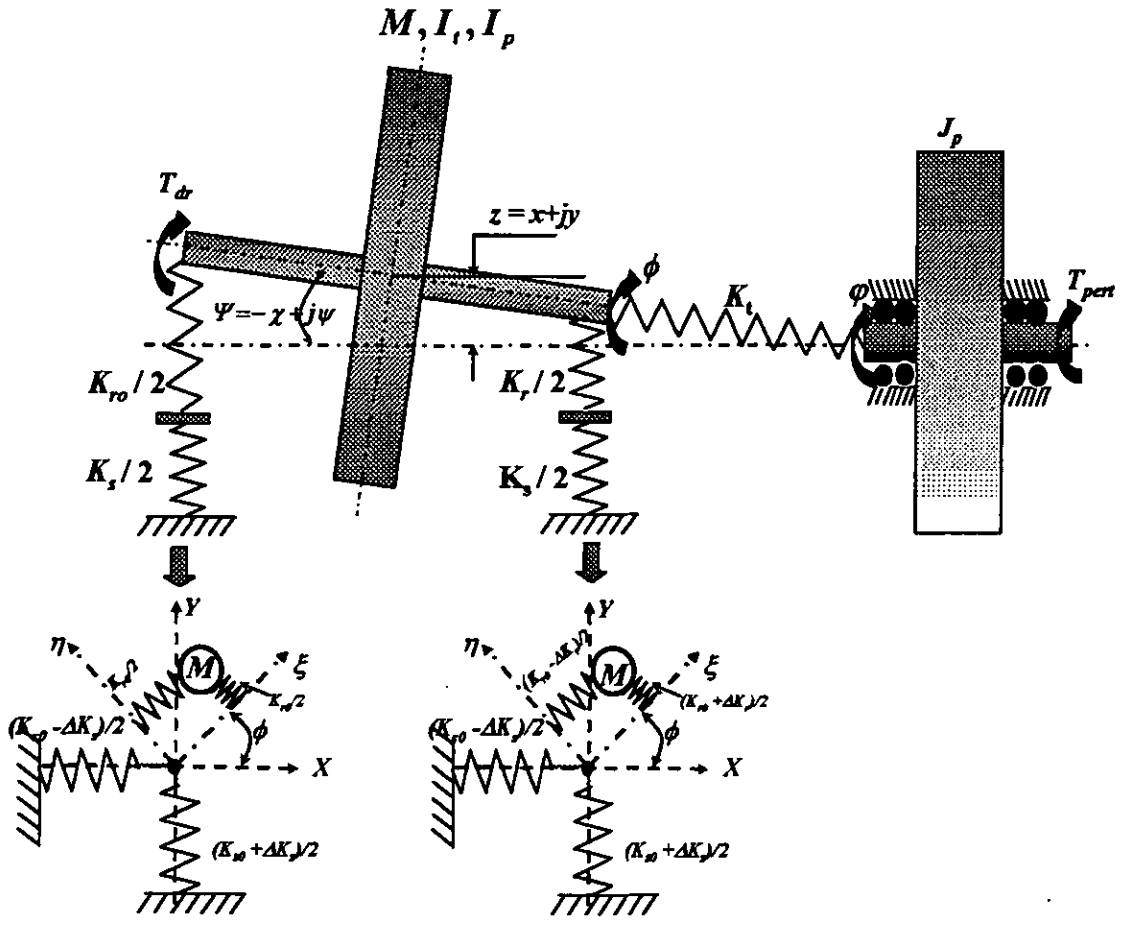

Figure 2. Physical model of the rotor.

The support stiffness is connected in sequence with rotating symmetric stiffness element with stiffness $K_{ro}/2$. The outboard end of the first rigid body is supported with the similar stationary stffness element, which is connected in sequence with the rotating stiffness element with major stiffness axes ξ and η and corresponding stiffnesses $K_{r0}\left[(1-\Delta)-\Delta K_r\right]/2$ and $K_{r0}\left[(1-\Delta)+\Delta K_r\right]/2$, where Δ and ΔK_r are overall stiffness reduction and stiffness asymmetry metry mesures. The second rigid body corresponds to the outboard disk D2 of the experimental rig (see Fig. 1). Asymmetry and average reduction of the rotating stiffness at the inboard end of the rotor represents the effect of a crack. The angle φ describes the second rigid body (see Fig. 2) the only torsional degree of freedom. It is associated with the torsional signal from the gear G_2. The torsional spring between these angles has stiffness $K_{t0}(1-\Delta_t)$, where Δ_t is an original torsional stiffness reduction due to the crack. The kinetic energy of the rotor system in Fig. 2 can be expressed as follows:

$$T=\frac{M}{2}\left(\dot{x}^2+\dot{y}^2\right)+\frac{I_p}{2}\left(\dot{\phi}^2-2\dot{\phi}\dot{\chi}\psi\right)+\frac{I_t}{2}\left(\dot{\chi}^2+\dot{\psi}^2\right)+$$
$$+\frac{J_p\dot{\varphi}^2}{2}+Ma\dot{\phi}\left[\dot{y}\cos(\phi+\delta)-\dot{x}\sin(\phi+\delta)\right] \qquad (1)$$

where M, I_p, I_t are correspondingly mass, polar and transverse moments of inertia of the inboard disk, J_p is the polar moment of inertia of the inboard disk, a, δ are polar coordinates of the mass center of the inboard disk expressed in the rotating frame. The potential energy of the system can be presented as follows:

$$\Pi = \frac{K_0}{2}\left[(1-d)\left(x^2+l^2\chi^2\right)+(1+d)\left(y^2+l^2\psi^2\right)-\frac{\Delta+q\cos 2\phi}{2}(x-l\chi)^2-\right.$$
$$\left.-\frac{\Delta-q\cos 2\phi}{2}(y+l\psi)^2-q(x-l\chi)(y+l\psi)\sin 2\phi\right]+\frac{K_{t0}(1-\Delta_t)(\phi-\varphi)^2}{2} \qquad (2)$$

where $K_0 = \frac{K_{r0}K_{s0}}{K_{r0}+K_{s0}}, q = \frac{\Delta K_r K_0}{K_{r0}^{\ 2}}, d = \frac{\Delta K_s K_0}{K_{s0}^{\ 2}}$, $2l$ is a distance between two plains of lateral response measurements P_1 and P_2. In addition to kinetic and potential energies the generalized forces affect the rotor system:

$$Q_x + jQ_y = P_0 e^{j\gamma} + Fe^{i\omega t} - D(\dot{x}+j\dot{y}),\quad -Q_\chi + jQ_\psi = -Dl^2(-\dot{\chi}+j\dot{\psi})$$
$$Q_\phi = T_{dr} - D_{t1}\dot{\phi},\quad Q_\varphi = -D_{t2}\dot{\varphi} + T_{t0} + T_{pert}\cos\omega_1 t \qquad (3)$$

where P_0, F are magnitudes of the constant radial force and nonsynchronous perturbation force, D is lateral damping evenly distributed between two supports of the inboard disk, D_{t1} and D_{t2} are torsional modal dampings, T_{dr} is a driving torque, T_{t0} and T_{pert} are constant and amplitude of harmonic components of torque created by the generator. After the introduction of the following nomenclature:

$$I_p = M\rho^2,\ I_t = \kappa^2 I_p,\ J_p = b^2 I_p,\ \nu_{l0} = \sqrt{\frac{K_0}{M}},\ n = \sqrt{\frac{K_{t0}M}{K_0 I_p}} = \frac{\nu_{t0}}{\nu_{l0}},$$
$$\varsigma = \frac{D}{2\sqrt{K_0 M}}, \varsigma_{t1} = \frac{D_{t1}}{2\sqrt{K_{t0}I_p}}, \varsigma_{t2} = \frac{D_{t2}}{2\sqrt{K_{t0}J_p}},\ L = \frac{l}{\kappa\rho},\ m = \frac{\Omega}{\nu_{l0}},$$
$$\sigma_{1,2} = \frac{\omega_{1,2}}{\nu_{l0}},\ p_0 = \frac{P_0}{\rho\kappa K_0},\ f_0 = \frac{F_0}{\rho\kappa K_0},\ \pi_{pert} = \frac{T_{pert}}{\rho^2 b^2 K_0}, \mu = \frac{a}{\kappa\rho} \qquad (4)$$

and new variables:

$$\phi = \tau+\beta_1-\beta_2,\ \varphi = \tau+\varphi_0+\beta_1+\beta_2,\ \tau = \Omega t,\ (...)' = \frac{d(...)}{d\tau},\ h = \frac{x+jy}{\kappa\rho}e^{-j\tau},\ \theta = (-\chi+j\psi)e^{-j\tau} \qquad (5)$$

the equations of motion can be written as follows:

$$h'' + 2(\varsigma+jm)h' + \left(1-\frac{\Delta}{2}-m^2+2jm\varsigma\right)h - \frac{q}{2}\bar{h} = \mu m^2 e^{j\delta} + p_0 e^{-jm\tau} + fe^{j(\sigma_1-m)\tau} + de^{-2jm\tau}\bar{h} + H$$
$$\theta'' + \left[2\varsigma L^2 - jm\left(\frac{1}{\kappa}-2\right)\right]\theta' + \left[L^2 - m^2 + jm\left(2\varsigma L^2 - j\frac{m}{\kappa^2}\right)\right]\theta = \frac{\Delta L}{2}h + \frac{qL}{2}\bar{h} \qquad (6)$$
$$\beta_1'' + 2\varsigma_t n\beta_1' = \frac{\pi_{pert}}{2}\cos\sigma_2\tau + \Phi,\ \beta_2'' + 2\varsigma_t n\beta_2' + 2n^2(1-\Delta_t)\beta_2 = \frac{\pi_{pert}}{2}\cos\sigma_2\tau - \Phi$$

where $\bar{h} = \frac{x-jy}{\kappa\rho}$, $j = \sqrt{-1}$

$$H = \mu e^{j\delta}\left[2m\left(\beta_1' - \beta_2'\right) + jm^2(\beta_1-\beta_2) - jn^2\beta_2\right] = O(\varepsilon^2)$$
$$\Phi = \frac{j\mu\kappa^2}{4}\left(\bar{h}e^{j\delta} - he^{-j\delta}\right) + \frac{\mu p_0}{2}\sin(m\tau+\delta-\gamma) + \frac{\mu f}{2}\sin(m\tau+\delta-\sigma_1\tau) = O(\varepsilon^2) \qquad (7)$$

Here ε is a measure of smallness and all terms of the third order are neglected.

To simplify the separation of torsional modes it was assumed that $b = 1$, $\varsigma_{t1} = \varsigma_{t2} = \varsigma_t$, although the introduction of normal coordinates for uncoupled torsional equations leads to similar equations in general case. The other assumptions are as follows:

$$\Delta,\ \Delta_t, q, \mu, f, p_0, \pi_{pert}, \varsigma, \varsigma_t \equiv O(\varepsilon) \tag{8}$$

As a consequence from the assumption (8) the following estimations can be made:

$$h, \beta_1, \beta_2 \equiv O(\varepsilon), \quad \theta \equiv O(\varepsilon^2) \tag{9}$$

The system of Eqs. (6) has been derived on the bases of relations (8), (9) with an accuracy up to the second order of smallness. It is important to note that within the consideration of terms up to the second order of smallness the terms H and Φ (Eqs. (7)) do not include crack-related information and can be exluded from further considerations. The rest of the system of Eqs. (6) can be treated by the method of Lapunov- Poincare. The solution in original variables can be expressed as follows:

$$x + jy = \begin{cases} \dfrac{M a \Omega^2}{DS(\Omega)} e^{j(\Omega t+\delta)}\left[1+\dfrac{K_0 q}{2\overline{DS}(\Omega)} e^{-2j\delta}\right] + \dfrac{M a \Omega^2}{\overline{DS}(\Omega)} \dfrac{K_0 d}{\overline{DS}(\Omega)} e^{-j(\Omega t+\delta)} \text{ - unbalance response} \\ \dfrac{P_0 e^{j\gamma}}{K_0(1-\Delta/2)}\left[1+\dfrac{K_0 q}{2DS(2\Omega)} e^{2j(\Omega t-\gamma)} + \dfrac{K_0 d}{\overline{DS}(2\Omega)} e^{-2j(\Omega t+\gamma)}\right] \text{ - radial load response} \\ \dfrac{F_0 e^{i\omega_1 t}}{DS(\omega_1)} + \dfrac{F_0}{\overline{DS}(\omega_1)} \dfrac{K_0 q}{2DS(2\Omega-\omega_1)} e^{j(2\Omega-\omega_1)t} + \\ \qquad + \dfrac{F_0 e^{-i\omega_1 t}}{\overline{DS}(\omega_1)} \dfrac{K_0 d}{\overline{DS}(\omega_1)} \text{ - nonsynchronous perturbartion response} \end{cases}$$

$$-\chi + j\psi = \begin{cases} \dfrac{M a \Omega^2 l}{PDS(\Omega,\Omega)} e^{j(\Omega t+\delta)}\left[\dfrac{K_0 \Delta}{2DS(\Omega)} + \dfrac{K_0 q}{2\overline{DS}(\Omega)} e^{-2j\delta}\right] \text{ - unbalance response} \\ \dfrac{P_0 e^{j\gamma}}{2K_0(1-\Delta/2)}\left[\dfrac{\Delta}{l} + \dfrac{K_0 q l}{2PDS(\Omega,2\Omega)} e^{2j(\Omega t-\gamma)}\right] \text{ - radial load response} \\ \dfrac{F_0 e^{i\omega_1 t}}{2DS(\omega_1)} \dfrac{K_0 \Delta l}{PDS(\Omega,\omega_1)} e^{i\omega_1 t} + \\ \qquad + \dfrac{F_0}{2\overline{DS}(\omega_1)} \dfrac{K_0 q l}{PDS(\Omega,2\Omega-\omega_1)} e^{i(2\Omega-\omega_1)t} \text{ - nonsynchronous perturbation response} \end{cases} \tag{10}$$

$$\beta_1 = \frac{1}{2}\mathrm{Re}\left[\frac{T_{pert} e^{j\omega_2 t}}{RTDS(\omega_2)}\right];\ \beta_2 = \frac{1}{2}\mathrm{Re}\left[\frac{T_{pert} e^{j\omega_2 t}}{TTDS(\omega_2)}\right]$$

where the following dynamic stiffness components are included

$$DS(\omega) = K_0(1-\Delta/2) - M\omega^2 + jD\omega;\ PDS((\Omega,\omega) = K_0 l^2 - \omega^2 I_t + \Omega\omega I_p + jDl^2\omega;$$
$$RTDS(\omega) = -I_p\omega^2 + jD_t\omega;\ TTDS(\omega) = 2K_{t0}(1-\Delta_t) - I_p\omega^2 + jD_t\omega \tag{11}$$

The torsional response could also include synchronous components if they are present in driving and/or load torque. The other torsional components such as laterally driven synchronous components,"snapping action" (see Bently et. al. (1997)) are small under the current set of assumptions. As expected the rigid body torsional dynamic stiffness (*RTDS*) is not affected by the crack, while the dynamic stiffness of the twisting torsional mode (*TTDS*) is affected. That dictates the necessity of subtracting the results of one plain torsional measurement from another for the rotor crack detection.

Considering rotor lateral response to the unbalance, it is important to note that rotating stiffness asymmetry introduced by the crack manifested in the sensitivity of the 1x forward component to the angular location of unbalance, while the support stiffness asymmetry is reflected in the 1x reverse component.

The rotor response to the radial load includes forward 2x component due to the rotating stiffness asymmetry, and reverse 2x component due to the support stiffness asymmetry.

The nonsynchronous perturbation actually separates response due to the support asymmetry from that due to the rotating stiffness asymmetry: the former relates to the reverse component with frequency of perturbation, while the latter is responsible for the component with frequency $2\Omega - \omega_1$.

It is important to note that the approximate solution (10) of the system of equations (6) is valid only if stable. Although the study of stability is outside the scope of this paper, it can be noted that the generating approximation of the system (6) has an instability zone in the proximity of the undamaged rotor translation mode resonance: $1 - \Delta/2 - q/2 < m < 1 - \Delta/2 + q/2$ (see, for example, Muszynska (1982) for similar results). In this narrow rotative speed range (rotating stiffness asymmetry parameter q is considered small) the solution (10) is not valid. The term with time-varying coefficient in the first of Egs. (6) has the second order of smallness and, therefore, can only slightly influence the boundaries of instability zone, defined by the generating approximation. Outside of the specified instability zone the solution (10) provided by the method of small parameter has accuracy up to the order of small parameter (see Giacaglia (1972)).

One of the important consequences of the expressions (10) is that the ratio of lateral rotor response z_2 measured at location P_2 to the lateral rotor response z_1 measured at location P_1 (Fig. 1) appeared to be very sensitive to the crack. Filtered to 1x components this ratio can be expressed as follows:

$$\left(\frac{z_2}{z_1}\right)_{1x} = \frac{\left[z + l(-\chi + j\psi)\right]_{1x}}{\left[z - l(-\chi + j\psi)\right]_{1x}} \approx 1 + \frac{K_0 l^2 \left(\Delta + qe^{-2j\delta}\right)}{K_0 l^2 - \Omega^2 \left(I_t - I_p\right) + jDl^2\Omega} \tag{12}$$

Note that the angular variable $-\chi + j\psi$ is measurable only by its contribution into the lateral displacements at different axial locations. The ratio in Eq. (12) characterizes the mode shape change due to the crack and is easy to measure. In the case of this ratio calculated for the nonsynchronous components, it will only include term related to the overall stiffness reduction:

$$\left(\frac{z_2}{z_1}\right)_{\omega_1} = \frac{\left[z + l(-\chi + j\psi)\right]_{\omega_1}}{\left[z - l(-\chi + j\psi)\right]_{\omega_1}} \approx 1 + \frac{K_0 l^2 \Delta}{K_0 l^2 - I_t \omega_1^2 + I_p \Omega \omega_1 + jDl^2 \omega_1} \tag{13}$$

From the experimental point of view the lateral dynamic stiffness of the translational mode (mode determined by the displacement of the mass center) for the forward component in relation to the direction of excitation force rotation (*FDS*) can be expressed as follows:

$$FDS_{1x} = \frac{2Ma\Omega^2 e^{j\delta}}{\left(z_1 + z_2\right)_{1x}} \approx K_0\left(1 - \frac{\Delta + qe^{-2j\delta}}{2}\right) - M\Omega^2 + jD\Omega$$

$$FDS_{\omega_1} = \frac{2F_0}{\left(z_1 + z_2\right)_{\omega_1}} \approx K_0\left(1 - \frac{\Delta}{2}\right) - M\omega_1^2 + jD\omega_1 \tag{14}$$

while the lateral dynamic stiffness of the translational mode for the reverse component (*RDS*) is determined by the relations

$$RDS_{-1x} = \frac{2Ma\Omega^2 e^{-j\delta}}{\left(z_1 + z_2\right)_{-1x}} \approx \frac{\left[K_0\left(1 - \frac{\Delta}{2}\right) - M\Omega^2 - jD\Omega\right]^2}{K_0 d}$$

$$RDS_{-\omega_1} = \frac{2F_0}{\left(z_1 + z_2\right)_{-\omega_1}} \approx \frac{\left[K_0\left(1 - \frac{\Delta}{2}\right) - M\omega_1^2 - jD\omega_1\right]^2}{K_0 d} \tag{15}$$

3. EXPERIMENTAL RESULTS

The experimental results are presented according to the types of excitation applied to the rotor system. The results of excitation of the rotor system with undamaged midspan section are compared with that obtained for the midspan with the transverse crack. The crack was created by applying a cycling load to the cantilever beam with a V-shaped stress concentrator. After the crack had developed the part of the cantilever beam with crack was cut and

installed as a midsection of the rotor rig (see Fig. 1). The approximate depth of the crack is 10%. It has been determined by analyzing the photographic pictures of the crack made under the microscope. Since the duration of the experiment was short in comparison with the duration of load cycling to create the crack, it is assumed that the crack depth has not changed during the experiment. The actual position of the crack in the rotor rig was chosen as closed to the undamaged rotor antinodal point as possible. According to the analytical investigation presented in the paper by Goldman et. al. (1996) the axial crack location at the antinodal point allows for the maximum sensitivity to the crack of that particular mode. The actual crack axial position in the experimental setup has an estimated sensitivity of 80% relative to that at the antinodal point.

3.1 TORSIONAL NONSYNCHRONOUS EXCITATION

As it was described above, the modification of the electric generator field using harmonic output of the function generator provides nonsynchronous torsional perturbation of the rotor. The resulting resistance torque has a harmonic component. Sweeping the frequency of the function generator and measuring the torsional response at the gears G_1 to G_4 the following parameters can be identified: perturbation torque=$(G_2-G_1)K_c$ (K_c=211 lb in/deg is a torsional stiffness of the reduced diameter shaft between gears G_2 and G_1), torsional compliance of the main rotor = $(G_3-G_4)_\omega/(G_2-G_1)K_c$ (a ratio of dynamic twist angle between 1 plains of torsional measurements G_3 and G_4 filtered to the torsional perturbation frequency, to the input perturbation torque) and torsional twist dynamic stiffness (*TTDS*)=1/(torsional compliance of the main rotor). The data is presented in the Bode plot format and dynamic stiffness format (Figure 3). The comparison of the torsional compliance and dynamic stiffness of the main rotor in undamaged case with that for the case of the rotor with crack shows the resonance frequency reduction on about 3% while the torsional stiffness reduction is about 40% (it shows a stiffening effect of the rotor system for high amplitudes at the resonance), with significant damping reduction. In the case of high radial force the lateral rotor response shows a component with torsional nonsynchronous perturbation frequency (Figure 4).

3.2 LATERAL NONSYNCHRONOUS EXCITATION

The nonsynchronous lateral excitation is provided by the constant force perturbator based on the constant elastic eccentricity, which is rotated by its own drive. Perturbation is performed in the direction of rotation. The lateral response measured at two axial locations P_1 and P_2 is filtered to the perturbation frequency. The resulting elliptic orbits are separated into the forward (in the direction of perturbation), and reverse (in the direction opposite to the perturbation) components. This process is referred to as a directional filtering. As it was shown in the analytical part only forward components are related to the rotor crack, while reverse components are caused by the support asymmetry. The average of two forward components, measured at location P_1 and location P_2 represents the translational motion of the inboard disk. This data in the format of Bode plot and dynamic stiffness is shown in Fig. 5. Note that the difference in the lateral resonance frequencies between undamaged and cracked rotors is about 1% while actual reduction of the lateral stiffness is 15%.

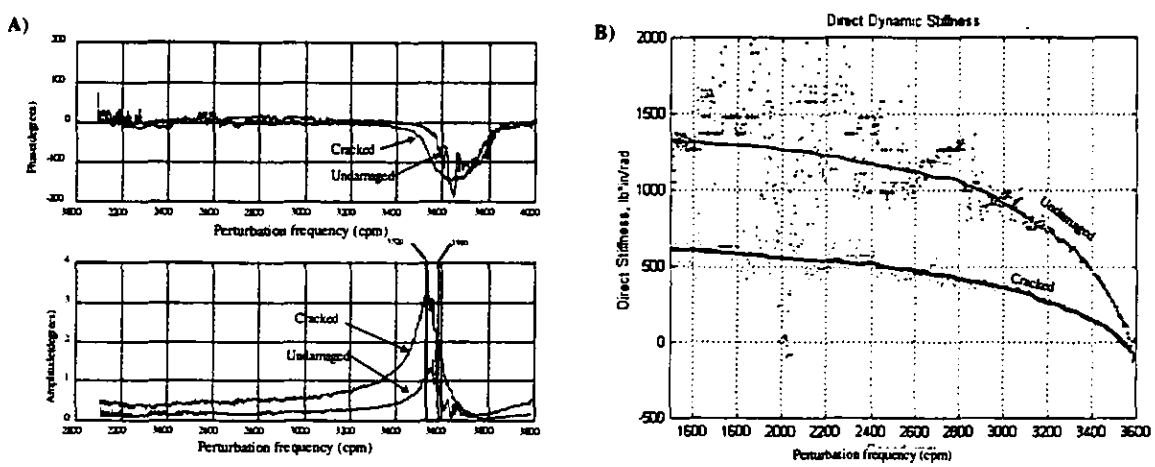

Figure 3. Torsional compliance (A) and direct dynamic stiffness (B) of the main rotor with and without crack at Ω=2000 rpm. The direct stiffness approximation as a parabola according to Eq. (11) gives the following numbers: $2K_{t0} = 1400\ \text{lb} \bullet \text{in} / \text{rad}$, $\Delta_t = 0.4$.

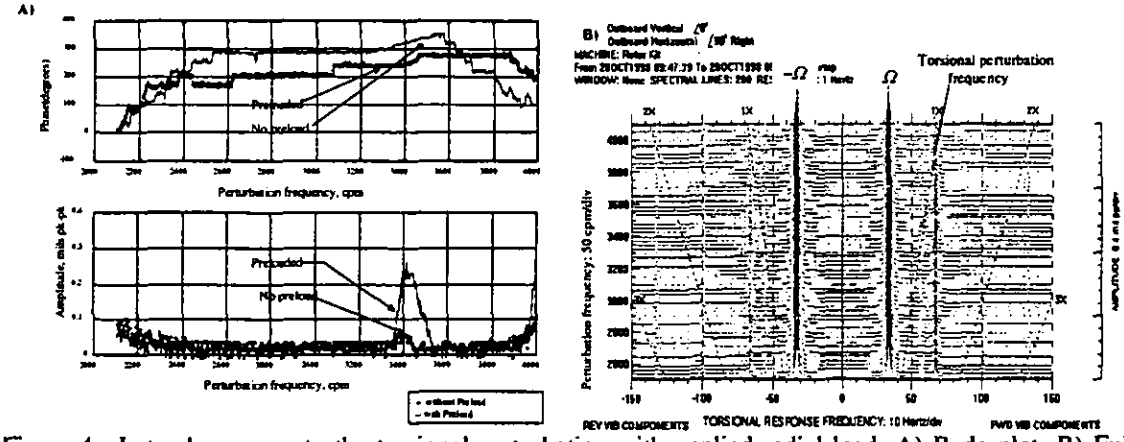

Figure 4. Lateral response to the torsional perturbation with applied radial load: A) Bode plot, B) Full spectrum cascade. Note the cross-coupling apperance under the radial load conditions.

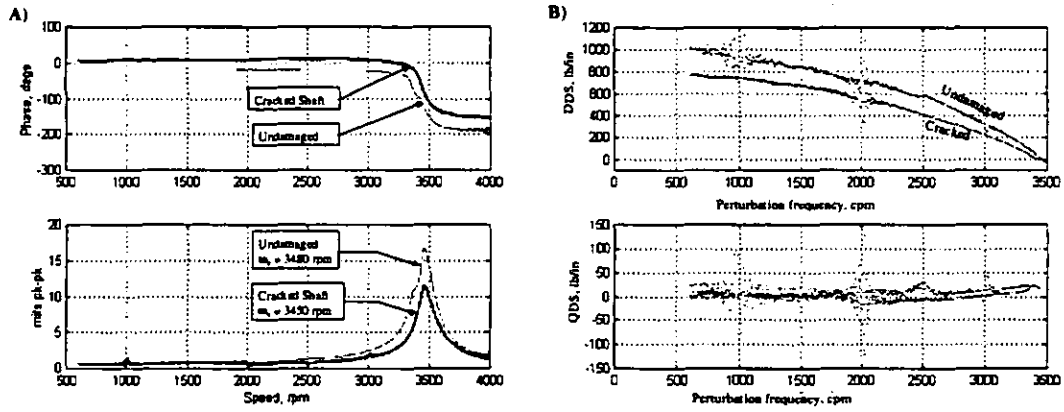

Figure 5. Forward component of the lateral response of the inboard disk mass center to lateral forward nonsynchronous perturbation (A) and dynamic stiffness of the main rotor FDS_{ω_1} (B) with and without crack. The direct stiffness approximation as a parabola according to Eq. (11) gives the following numbers: $K_0 = 930$ lb / in, $\Delta = 0.15$.

4. CONCLUSIONS

The analytical and experimental results presented above lead to the following conclusions:

- The rotor crack manifests in changes of the forward components of lateral response filtered orbits (1x filterd in the case of synchronous excitation, filtered to the perturbation frequency in case of nonsynchronous lateral perturbation). The reverse components are related to the support stiffness asymmetry. This makes directional filtering an effective data processing technique for early crack detection. The results of directional filtering can be presented in full spectrum format.

- Due to nonlinearities of the rotor system at high lateral and torsional amplitudes and possible instabilities the resonance frequencies are not very sensitive to the rotor crack. The dynamic stiffness identification procedure allows identifying lateral and torsional stiffness, which exhibit much higher sensitivity to the crack. Torsional mode is affected more then lateral mode.

- The analytical results show the sensitivity of the mode shape to the crack. Under the different set of assumptions this sensitivity was also analytically investigated in Goldman et. al. (1996). This result requires further experimental investigation. The sensitivity of the modal lateral rotor response to the crack axial location and its depth has been at least analytically studied, while the torsional modes sensitivity to the crack is almost completely unknown.

- From the practical application stand point the information on the mode shapes and dynamic stiffness can be obtained by differential data processing from the original start up and that with the trial weight. The result is usually presented as an influence vector. It is reciprocal to the synchronous dynamic stiffness. As it is stated above only forward components of lateral response have to be taken into account. The ratio of the influence vectors at different rotor axial locations can be used as a mode shape inicator.

NOMENCLATURE

a, δ	polar coordinates of inboard disk mass center in rotating frame
$b^2=I_t/I_p$, $\kappa^2=J_p/I_p$	transversal inboard and outboard disks moments of inertia ratios
D, D_{t1}, D_{t2}	lateral and torsional damping at inboard and outboard disks
d, q	lateral stationary and rotating stiffness asymmetry parameters
$DS(\omega)$	lateral dynamic stiffness of translational mode
$Fe^{j\omega t}$	nonsynchronous lateral excitation force
FDS	lateral dynamic stiffness for the translational mode forward component
h	nondimensional lateral displacement vector
J_p	outboard disk polar moment of inertia
l	half length of the first rigid body
K_0	original total lateral stiffness of the rotor/bearing system at the inboard disk location
K_{r0}	lateral rotating stiffness of undamaged rotor
$(K_{s0}\pm\Delta K_s)/2$	lateral stationary support stiffness in major stiffness axes X and Y
K_{t0}	torsional stiffness of the undamaged rotor
L	nondimensional half length of the first rigid body
m, n	rotative speed and torsional natural frequencies ratios
M, I_p, I_t	Mass, polar and transversal moment of inertia of the inboard disk
PDS	lateral dynamic stiffness of the pivotal mode
$P_0e^{j\gamma}$	constant radial load
p_0, f_0, π_{pert}	nondimensional magnitudes of constant radial load, nonsynchronous lateral and torsional perturbations
Q_x, Q_y, Q_χ, Q_ψ	generalized forces
RDS	lateral dynamic stiffness for the translational mode reverse component
$RTDS$	torsional dynamic stiffness for the rigid body mode
T_0	constant component of the resistance torque
T_{dr}	driving torque
$T_{pert}\cos\omega t$	torsional nonsynchronous perturbation torque
$TTDS$	torsional dynamic stiffness for the twisting mode
$z=x+jy$	first rigid body center of mass lateral displacement vector
β_1, β_2	modal coordinates for torsional rigid body and twisting modes
Δ	average rotor lateral stiffness reduction parameter
Δ_t	torsional stiffness reduction parameter
ΔK_r	rotating stiffness asymmetry due to the crack
ε	measure of the order of smallness
ζ, ζ_{t1}, ζ_{t2}	lateral and torsional inboard and outboard disks damping factors
η, ξ	rotating strong and weak major stiffness axes of the cracked rotor
$\theta=-\chi+j\psi$	angular displacement vector combined from the angle χ of yaw and angle ψ of pitch
μ	nondimensional eccentricity of the first rigid body center of mass
υ_{t0}, υ_{t0}	lateral and torsional natural frequencies of undamaged rotor
ρ	gyration radius of inboard disk
$\sigma_{1,2}$	lateral and torsional perturbation frequencies ratios
τ	nondimensional time

LITERATURE

1. Bently, D. E., Muszynska, A., "Detection of Rotor Cracks", Proceedings of 15th Turbomachinery Symposium, Corpus Christi, Texas, Nov. 1986, pp. 129-139.
2. Bently, D. E., Goldman, P., Muszynska, A, ""Snapping" Torsional Response of an Anisotropic Radiallly Loaded Rotor", ASME TURBO EXPO 1995, Transactions of ASME, Journal of Engineering for Gas Turbines and Power, v. 119, No. 2, 1997
3. Chen, W. H., Wang, H. L., "Finite element analysis of axisymmetric cracked solid subjected to torsional loadings", Eng. Frac. Mech., vol. 23, No 4, 1986, pp. 705-717.
4. Christides, S., Barr, A. D. S., "Torsional vibration of cracked beams of non-circular cross-section", Int. J. Mech. Sci., vol. 28, No 7, 1986, pp. 473-490.
5. Cohen, R., Porat,I., "Coupled Torsional and Transverse Vibration of Unbalanced Rotor", J. of Applied Mechanics, 1985, vol. 52, No 9, pp. 701-705.
6. Dimarogonas, A. D., Papadopoulos, C. A., "Vibration of cracked shafts in bending", J. Sound Vib., Vol. 91, 1983, pp. 583-593.
7. Dimarogonas, A. D., Massouros, G., "Torsional vibration of a shaft with circumferential crack", Eng. Frac. Mech., vol. 15, No 3-4, 1981, pp. 439-444.
8. Dimentberg, F. M., "Flexural Vibration of Rotating Shafts", Butterworth, London, 1961.
9. Dirr, B. O., Schmalhorst, B. K., "Crack depth Analysis of a Rotating Shaft by Vibration Measurement", 11th ASME Conf. Vib. Noise, Boston, DE v. 2, 1987, pp. 607-614.
10. Giacalglia, G. E. O., "Perturbation Methods in Non-Linear Systems", Springer-Verlag, New York, 1972, 319 pp.
11. Gasch, R., "Dynamic behavior of a simple rotor with a cross-sectional crack", Vibrations in Rotating Machinery, Inst. of Mech. Eng., London, 1976, pp. 123-128.
12. Goldman, P., Bently, D. E., Muszynska, A., "The Modal Diagnostics of Rotors with Cracks", International ME 96 Congress and Exhibition, November 1996, Atlanta, Georgia, USA.
13. Grabowski, B., "The vibrational behavior of a turbine rotor containing a transverse crack", J. Mech. Des., vol. 102, 1979, pp. 15-19.
14. Henry, T. A., Okah-Avae, B. E., "Vibrations in cracked shafts", Vibrations in Rotating Machinery, Inst. of Mech. Eng., London, 1976, pp. 15-19.
15. Inagaki, Y., Kanaki, H., Shiraki, K., "Transverse Vibrations of a General Cracked Rotor Bearing System", ASME Paper 81-DET-45, 1981.
16. Mayes, I. W., Davies, W. G. R., "The Vibrational Behavior of a Rotating Shaft System Containing a Transverse Crack", I. Mech. E. Conference, Paper C178/76,1976.
17. Muszynska, A., "Shaft Crack Detection", Seventh Machinery Dynamics Seminar, Canada, 1982.
18. Muszynska, A., Goldman, P., Bently, D. E., "Torsional /lateral Cross-Coupled Responses Due to Shaft Anisotropy: A new Tool in Shaft Crack Detection", IMechE, C 432-090, Bath, United Kingdom, 1992.
19. Nelson, H. D., Nataraj, C., "The Dynamics of a Rotor System with a Cracked Shaft", ASME J. Vibration, Acoustics, Stress and Reliability in Design, vol. 108, No 2, 00. pp. 189-196.
20. Papadopoulos, C. A., Dimarogonas, A. P., "Coupled Vibration of Cracked Shafts", Rotating Machinery Dynamics, ASME, DE-Vol. 18-2, 1989, pp. 7-12.
21. Qian, G., Gu, S., Jiang, J., "Finite element model of cracked plates application to vibration problem", Comput. Str., 39, 5, 1991, pp. 483-487.